Organization and somatotopy of corticothalamic projections from L5B in mouse barrel cortex

Anton Sumser[a,b,c,d,1], Rebecca A. Mease[a,d], Bert Sakmann[a,c,1], and Alexander Groh[a,d]

[a]Institute for Neurosciences, Technische Universität München, 80802 Munich, Germany; [b]Graduate School of Systemic Neurosciences, Ludwig-Maximilians Universität München, 82152 Martinsried, Germany; [c]Research Group Cortical Column in Silico, Max Planck Institute for Neurobiology, 82152 Martinsried, Germany; and [d]Department of Neurosurgery, Technische Universität München, 81675 Munich, Germany

Contributed by Bert Sakmann, July 10, 2017 (sent for review March 21, 2017; reviewed by David Fitzpatrick, Michael Frotscher, and Jeff W. Lichtman)

Neurons in cortical layer 5B (L5B) connect the cortex to numerous subcortical areas. Possibly the best-studied L5B cortico–subcortical connection is that between L5B neurons in the rodent barrel cortex (BC) and the posterior medial nucleus of the thalamus (POm). However, the spatial organization of L5B giant boutons in the POm and other subcortical targets is not known, and therefore it is unclear if this descending pathway retains somatotopy, i.e., body map organization, a hallmark of the ascending somatosensory pathway. We investigated the organization of the descending L5B pathway from the BC by dual-color anterograde labeling. We reconstructed and quantified the bouton clouds originating from adjacent L5B columns in the BC in three dimensions. L5B cells target six nuclei in the anterior midbrain and thalamus, including the posterior thalamus, the zona incerta, and the anterior pretectum. The L5B subcortical innervation is target specific in terms of bouton numbers, density, and projection volume. Common to all target nuclei investigated here is the maintenance of projection topology from different barrel columns in the BC, albeit with target-specific precision. We estimated low cortico–subcortical convergence and divergence, demonstrating that the L5B corticothalamic pathway is sparse and highly parallelized. Finally, the spatial organization of boutons and whisker map organization revealed the subdivision of the posterior group of the thalamus into four subnuclei (anterior, lateral, medial, and posterior). In conclusion, corticofugal L5B neurons establish a widespread cortico–subcortical network via sparse and somatotopically organized parallel pathways.

somatotopy | corticothalamic projections | whisker system | posterior medial thalamic nucleus | thalamus

A common feature of sensory systems is the topographic organization of their ascending pathways from the sensors to the cortex. A prominent example of topographic projections is the rodent whisker system in which the arrangement of whisker follicles on the snout of the animal is mapped at each synaptic station up to the cortex, where the whisker map forms the cortical barrel field of rodents (1). Although this strict topographic organization is well established for the ascending pathway (2), the extent to which this map organization continues beyond the primary somatosensory cortex via descending projections to subcortical structures is less clear.

One major target of descending cortico-efferent projections is the thalamus, which is innervated by two distinct corticothalamic pathways. First, neurons in cortical layer 6 (L6) provide numerically large and somatotopically organized (3) feedback to the sensory thalamus. Secondly, layer 5B thick-tufted neurons (L5B) innervate exclusively higher-order thalamus with sparse but uniquely large driver synapses and unclear somatotopic organization (3–5). Probably the best-characterized example of a L5B target nucleus is the lateral part of the posterior group (PO) in the thalamus (POm), where cortical L5B neurons provide the dominant synaptic input (6, 7). Receptive field studies support somatotopic organization of the POm even though an anatomical whisker map has not been shown (8). L5B neurons also project to the ventral thalamus, midbrain, and brainstem (4, 5), but the organization of their projection fields is unknown. Here we investigated by quantitative anatomy whether cortico–subcortical projections to the thalamus and anterior midbrain are somatotopically organized.

We labeled barrel cortical boutons by dual-color anterograde tract tracing to reconstruct the 3D location of giant L5B boutons in the entire thalamus and the anterior midbrain. We found discrete bouton clouds in four areas of the dorsal thalamus, one in the ventral thalamus (zona incerta, ZI), and another in the anterior pretectum (APT). L5B projections to each of these areas were somatotopically arranged, thereby mapping the whisker pad to subcortical areas. The somatotopic precision, map orientation, and numbers of boutons were target-area specific and revealed the subdivision of the PO into four distinct L5B target nuclei.

Results

Labeling of L5B Neurons and Boutons. We labeled cortico–subcortical boutons by depositing two different adeno-associated virus (AAV) constructs in the barrel cortex (BC) of seven mice (Fig. 1 *A*–*C* and Fig. S1). Transfected cells expressed the presynaptic marker Synaptophysin fused to either GFP or mOrange (Fig. 1*C*) (9). Deposits were targeted to L5 and labeled on average 91 [median; first quartile (Q_1): 50; third quartile (Q_3): 141] L5B neurons in 3 (Q_1: 2; Q_3: 4) barrel columns. Dual virus deposits were always nonoverlapping, with their borders being 260 μm apart (Q_1: 221 μm; Q_3: 355 μm; equivalent to approximately two barrel diameters). In mice, the interbarrel septa are much less prominent than in rats (10). Viral deposits included barrel and septal regions (Fig. S1), so putative barrel- or septal-specific projection patterns (11) could not be distinguished. Following fluorophore expression, we acquired images of the entire thalamus and adjacent midbrain regions via mosaic confocal fluorescence microscopy (Figs. 1 *D* and *E* and 2 *A*–*D* and Fig. S2). These images were used to reconstruct the position of giant synaptic boutons (Fig. 2 *E* and *F*). Only boutons with apparent diameters >1.5 μm were defined as giant boutons originating

Significance

In the somatosensory system, signals are transduced from peripheral sensors up to the cerebral cortex in a topographic manner, meaning that the relative spatial organization of the sensory receptors is represented by a map in the cortex. Because the somatosensory cortex is not the terminus of sensory signals, we investigated whether topographic maps are maintained beyond the cortex via cortical output pathways from thick-tufted layer 5B (L5B) neurons. We found that L5B neurons in the somatosensory cortex topographically target six separate subcortical nuclei with area-specific projection strength, map orientation, and topographic precision. Thus topographic organization persists beyond the primary cortex via the L5B pathway with target-specific precision.

Author contributions: A.S., B.S., and A.G. designed research; A.S. performed research; A.S. and R.A.M. analyzed data; and A.S., R.A.M., B.S., and A.G. wrote the paper.

Reviewers: D.F., Max Planck Florida Institute; M.F., University of Hamburg; and J.W.L., Harvard University.

The authors declare no conflict of interest.

[1]To whom correspondence may be addressed. Email: anton.sumser@lrz.tu-muenchen.de or bsakmann@neuro.mpg.de.

This article contains supporting information online at www.pnas.org/lookup/suppl/doi:10.1073/pnas.1704302114/-/DCSupplemental.

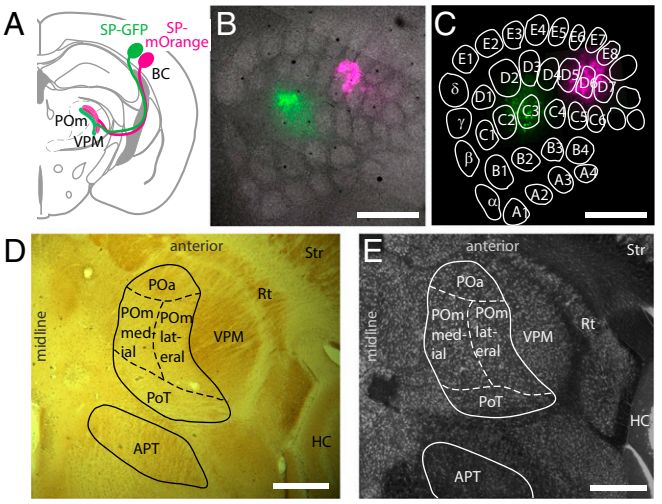

Fig. 1. Cortical bouton labeling and borders of subcortical target nuclei. Subcortical L5B boutons in the thalamus were labeled by virus-mediated expression of two different fluorescent proteins in barrel cortical neurons. (*A*) Schematic showing dual injection of viral particles encoding Synaptophysin–GFP (SP–GFP, green) and Synaptophysin–mOrange (SP–mOrange, magenta) into the BC and projections in the thalamus (modified from ref. 12). (*B*) Merged confocal fluorescence image of tangential sections of the BC at the level of layer 4, showing barrels (gray; Streptavidin staining) and deposits of SP–GFP (green) and SP–mOrange (magenta). (*C*) As in *B*, but at the L5B level with labeled L5B somata. Barrel outlines are from *B*. (*D*) Horizontal section (cytochrome c oxidase staining) containing L5B target nuclei in the thalamus: (POa, POm_{medial}, $POm_{lateral}$, PoT, and APT). The VPM, thalamic reticular nucleus (Rt), striatum (Str), and hippocampus (HC) are indicated for orientation. Zona incerta is shown in Fig. S1. (*E*) An image at a level similar to that shown in *D* but stained for neuronal somata by NeuroTrace. (Scale bars: 500 μm in *B*–*E*.)

from L5B neurons. Smaller boutons are from L6 and were ignored for the analyses (4). We thus generated 3D reconstructions of subcortical L5B bouton clouds in the entire thalamus and anterior midbrain (Fig. 2*G* and Movie S1).

Target Areas of L5B Neurons. Dual viral deposits in the BC (Fig. 3 *A* and *E*) labeled separate L5B bouton clouds in the thalamus and the anterior midbrain (Figs. 1 *D*–*E* and 3 *B*–*D* and *F*–*H* and Movie S1) as well as in the superior colliculus, pontine nuclei, and trigeminal nuclei. Using cytochrome c oxidase and NeuroTrace labeling (Figs. 1 *D* and *E* and 2*A*) allowed us to register the bouton clouds to the coordinates of the mouse brain atlas (12). We identified the following L5B target areas in the thalamus and the anterior midbrain: four spatially segregated clouds in the PO (Fig. 3 *B* and *F*), one in the ZI (Fig. 3 *C* and *G*), and another in the APT (Fig. 3 *D* and *H*). Table 1 lists the centroids of the bouton clouds for each of the reported nuclei in coronal mouse brain atlas-equivalent coordinates (12). We found that the four bouton clouds in the PO were arranged in the horizontal plane and together formed an ellipsoid (Fig. 3 *B* and *F*). Based on the cytoarchitecture corresponding to these clouds, we suggest that the PO can be subdivided into four subnuclei (Figs. 1 *D* and *E* and 2 *A*, *D*, and *E*). In accordance with established naming conventions, we refer to these four PO subnuclei as anterior PO (POa), $POm_{lateral}$, POm_{medial}, and PO, triangular part (PoT).

In contrast to earlier reports (13, 14), we found only weak or no labeling in the ventral posterior lateral nucleus (VPL). Furthermore, amid numerous small boutons (Fig. S3*C*) from L6 (4), we detected few large boutons in a posterior area of the ventral posterior medial thalamic nucleus (VPM) (Fig. S3*D*), as reported previously (15). However, the low numbers of large boutons (fewer than three boutons per labeled L5B neuron on average) in the VPM and VPL prevented detailed analyses.

Bouton Cloud Quantifications. We quantified bouton sizes and numbers, as well as volumes and densities of bouton clouds, in six target nuclei in the thalamus (four of which were within the PO) and anterior midbrain. L5B bouton median diameters were 2.6 μm when labeled with GFP and 2.9 μm when labeled with mOrange (no deconvolution was applied). Bouton diameters in the different target areas were comparable, and medians ranged between 2.3 and 2.9 μm with GFP labeling and between 2.6 and 3.2 μm with mOrange labeling (Fig. 4*A* and see Table 1 for quartiles).

We next estimated the average number of boutons supplied per labeled L5B neuron by normalizing bouton counts in the different nuclei by the number of fluorescently labeled somata in L5B for each experiment. Because not all neurons in L5B are projection neurons, the reported numbers of boutons are lower-bound estimates. The median number of giant boutons supplied by single labeled L5B neurons was highly variable across target areas and ranged between 5.8 and 29.5. According to these estimates, a single labeled L5B neuron supplies most boutons to the $POm_{lateral}$ and APT (median >24 boutons), whereas the ZI receives ≈18 boutons, and the POa, POm_{medial}, and PoT receive fewer than 10 giant boutons (see Fig. 4*B* and Table 1 for details). Normalizing bouton numbers by the ratio of the labeled column volume to the average column volume, we estimate that one column supplies ≈1,000 giant boutons to the $POm_{lateral}$ and APT and between 220 and 480 giant boutons to the other target nuclei (Table 1 and Fig. S4).

When approximating bouton cloud volumes per labeled L5B neuron in the respective nuclei, PO subnuclei (excluding the PoT) had the smallest cloud volumes, with fewer than 1.1e4 mm^3 per labeled L5B neuron, whereas in the PoT, APT, and ZI boutons were spread over significantly larger volumes (Fig. 4*C* and Table 1). As a measure of innervation density, we calculated bouton cloud densities in the respective targets. We found the highest bouton densities in the $POm_{lateral}$, with a median of 3.7e5/mm^3, significantly higher than in all other nuclei (Fig. 4*D* and Table 1). POm_{medial} bouton densities were intermediate (1.5e5/mm^3), whereas POa, PoT, and APT densities were below 1e5/mm^3 (Fig. 4*D* and Table 1). We further estimated soma densities based on a subset of experiments with NeuroTrace colabeling. We found comparable soma densities of ≈4.5e4/mm^3 in the PO and APT, similar to previous reports in the rat (16). In the ZI we estimated a lower density (2.2e4/mm^3) (Fig. 4*E* and Table 1).

The ratio between bouton density and soma density in the target area yielded an estimated average of available giant boutons per target neuron in the different nuclei (Fig. 4*F* and Table 1). In all subcortical target areas, individual neurons are estimated to receive few (<10) giant boutons. Neurons in the $POm_{lateral}$ were estimated to be targeted by approximately eight boutons, whereas neurons in all other analyzed areas receive significantly fewer boutons (fewer than four). In summary, L5B neurons innervate subcortical target nuclei sparsely with the strongest innervation in the $POm_{lateral}$.

Somatotopic Segregation. The reconstructed bouton clouds from the dual injections in the BC showed little overlap in the subcortical nuclei (e.g., Fig. 3*D*), suggesting somatotopic organization of the L5B cortico–subcortical projections. As a measure of somatotopic segregation, we estimated the degree of overlap between clouds with a generalized linear model (GLM) approach (17), which identifies and quantifies boutons in mixed-color areas (Fig. S5). In Fig. 5 *A* and *B* the GLMs are illustrated as the border surfaces between GFP- and mOrange-labeled bouton clouds. The advantage of the GLM approach compared with alternative volume and binning methods for measuring overlap is that the GLM approach is much less dependent on cloud shape, bouton density, or bin size. We found that bouton clouds overlapped to different degrees depending on the target nucleus. The POm (medial and lateral) and APT had median overlaps of 19–30%, whereas the POa, PoT, and ZI had overlaps of more than 40% (Fig. 5*C* and Table 1). The negative correlation between the border distance of the two deposits in the BC and the resulting subcortical overlap was significant in the $POm_{lateral}$ and APT ($P < 0.05$, Pearson correlation).

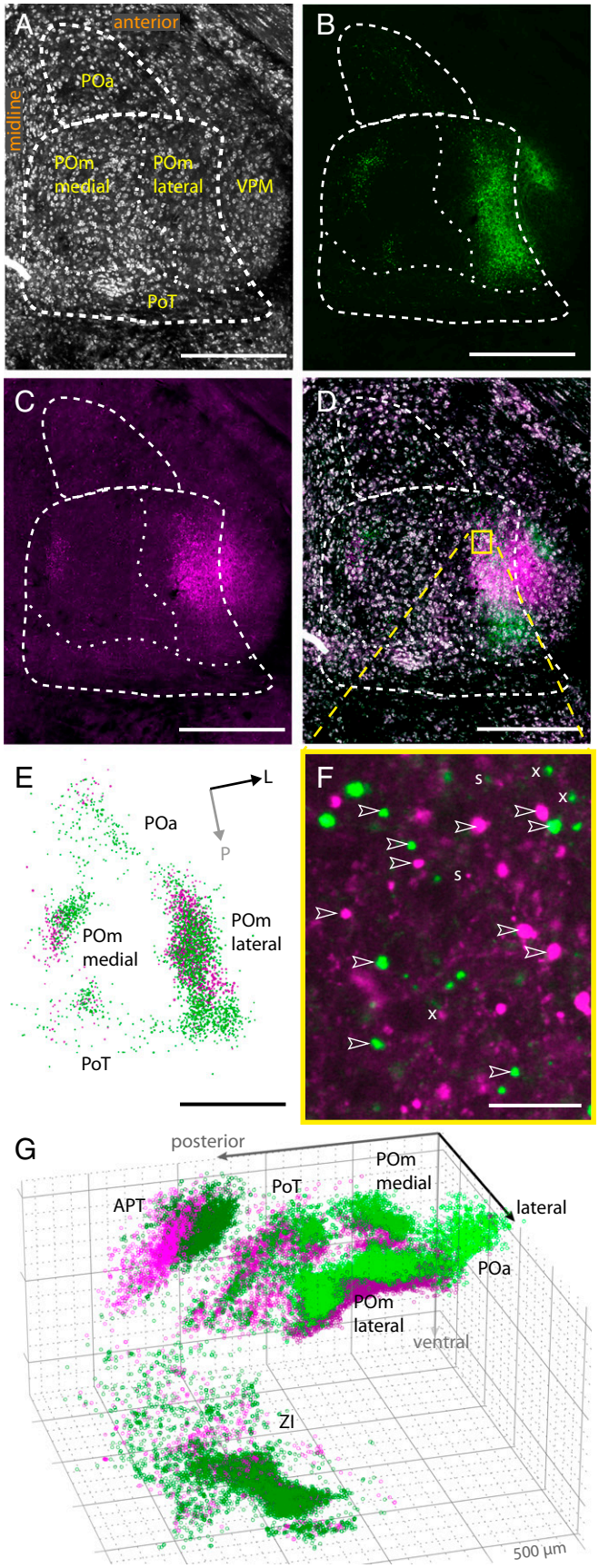

Fig. 2. Reconstructions of subcortical L5B bouton clouds. Shown are examples of confocal sections and bouton reconstructions. (*A*–*C*) Individual channels of horizontal sections through L5B target nuclei in the dorsal thalamus. (*A*) Somata (NeuroTrace staining; gray). (*B*) GFP-labeled L5B boutons (green). (*C*) mOrange-labeled L5B boutons (magenta). (*D*) Overlaid sections *A*–*C*. Dashed lines indicate borders of PO nuclei. (*E*) Reconstructed boutons from *B* and *C* (green and magenta, respectively). Bouton diameters are up-scaled twofold to increase visibility. Arrows indicate orientation (L, lateral; P, posterior). (*F*) Enlarged view of the boxed area in *D* but without the NeuroTrace signal. Arrowheads mark examples of putative giant L5B boutons (>1.5 µm). Small puncta (s, <1.5 µm) were excluded; "x" indicates examples of boutons that had their maximum brightness in an adjacent z-section. (*G*) 3D illustration of reconstructed boutons from experiments in *A*–*F*. Major grid lines are spaced by 500 µm. (Scale bars: 500 µm in *A*–*D* and *F*; 25 µm in *E*.)

In summary, L5B projections from neighboring areas in the BC to subcortical target nuclei are largely segregated with a varying degree of overlap depending on the subcortical target nucleus, indicating L5B cortico–subcortical somatotopic organization.

Whisker Projection Maps. Rowish (Fig. 3 *A*–*D*) and arcish (Fig. 3 *E*–*H*) dual virus deposits in the BC yielded different relative bouton cloud positions in the target nuclei, raising the possibility that the BC whisker map is projected to subcortical target nuclei via L5B projections. Therefore we tested if bouton cloud positions can be predicted from the relative positions of deposit sites in the BC. We fitted and evaluated linear regression models to the data, using the relative deposit locations in the barrel field as input and relative bouton cloud centroid locations in each target nucleus as output. $POm_{lateral}$ and APT bouton clouds could be predicted accurately (prediction SEM 2° for the $POm_{lateral}$ and 3° for the APT), and the prediction errors for the other nuclei were only slightly larger (6° for the Poa, 7° for the POm_{medial}, 9° for the PoT, and 5° for the ZI), indicating projection maps of L5B origin in the target nuclei.

Furthermore, using the fitted models to predict virtual purely rowish and arcish deposits, we estimated the individual barrel field projection map orientations in the thalamus and anterior midbrain (Table 1). In the four PO subnuclei, whisker arcs 1–7 are arranged from dorsal to ventral. In contrast, whisker rows A–E are organized concentrically from the outside to the center of the PO, e.g., in an anterior–posterior direction for the POa and in a lateral–medial orientation for the $POm_{lateral}$ (see the schematic in Fig. 6 and unit vector directions in Table 1). Notably, the center of the PO was always devoid of cortical giant boutons (Fig. S6), even when deposits included E row cortical columns that project to the innermost part of the PO. Finally, in the APT, projection rows A–E point posterolaterally, and arcs 1–7 point ventroposteromedially, whereas in the ZI the projection rows point anteroventrally, and arcs are oriented medially.

In summary, L5B inputs endow each target nucleus with an individually oriented somatotopic whisker map. In combination, the four whisker maps in the PO form a circular row structure from outside to inside and a homogeneous arc orientation in the dorsal-to-ventral direction.

Discussion

On anatomical grounds the POm is part of the whisker system, and POm cells are responsive to whisker deflections (2, 8, 18), but the function of the POm in whisker processing is still unclear (19, 20). The main synaptic drive of the POm originates in the BC in L5B (6, 7, 18). Anatomical and physiological properties point to the possibility of substructures in the PO, albeit not conclusively (21, 22). Here, using quantitative neuronal projection tracing, we found that L5B giant boutons cluster in four spatially segregated regions of the PO. Additionally, the ZI and APT—two regions that were shown to inhibit POm (23, 24)—receive substantial input from L5B. Two-color labeling of L5B boutons revealed that in each target area bouton clouds repeat the relative spatial arrangement of the whiskers on the animal's snout. Thus, descending L5B projections are somatotopically arranged into whisker maps with target-specific orientation.

NEUROSCIENCE

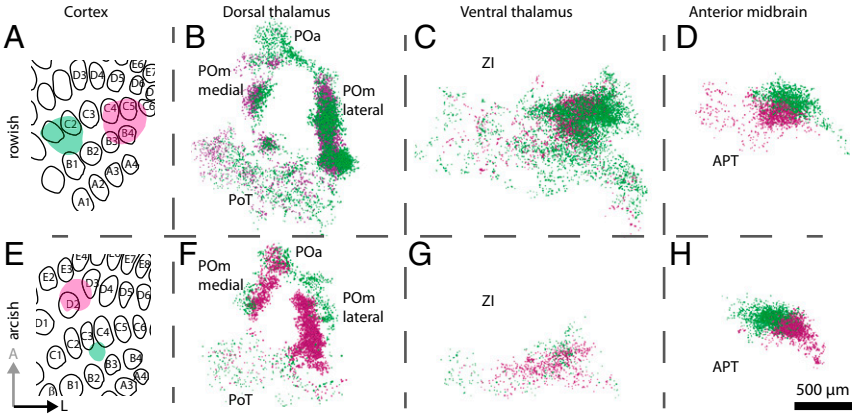

Fig. 3. Topology of cortico–subcortical projections. Two experiments with dual-color labeling (GFP, green, and mOrange, magenta) in the rowish (*A–D*) and arcish (*E–H*) direction resulted in different relative subcortical positions of bouton clouds. *B–D* and *F–H* are in horizontal orientation. (*A*) Rowish dual-color labeling in the BC approximately along the C row (green and magenta areas). (*B–D*) Reconstruction of bouton clouds (see the 3D illustration of subcortical bouton clouds in Fig. 2*G*) in the dorsal thalamus (PO; GFP-labeled boutons are located dorsally to mOrange-labeled boutons) (*B*), ZI (*C*), and APT (*D*). (*E*) As in *A*, but for an experiment with arcish dual-color labeling approximately along arcs 2–3 of the BC. (*F–H*) As *B–D* resulting from the dual-color labeling shown in *E*. (Scale bar: 500 µm.)

Methodological Considerations. We labeled the cortico–subcortical pathways from L5 and L6 in the mouse BC with Synaptophysin–fluorophore fusion proteins (25). Compared with L5 projections, L6 innervates the thalamus densely with small boutons (Fig. S3) (4). Here, we investigated the cortico–subcortical pathway from L5B by focusing on boutons with diameters >1.5 µm, thus ignoring L6 boutons. To do so, we optimized the imaging parameters for large boutons. The sparseness and size of L5B boutons allowed us to sample coarsely in the z-direction (optical sections spaced by 10 µm) and thereby image the whole brain. To counteract signal loss through z-undersampling, we increased the size of the pinhole. With this low-resolution imaging approach, individual L6 boutons either were not resolved and appeared as regions with high background because of their high density and small size (Fig. S3) (4) or were excluded from the analyses because of their small diameter (<1.5 µm).

Subdomains in the PO. Bouton cloud reconstructions revealed four distinct L5B input areas in the dorsal thalamus, which together form an ellipsoid in the horizontal plane. The $POm_{lateral}$, POm_{medial}, and posterior (PoT) (12, 22) target areas are clearly within the PO. Based on Paxinos and Franklin's mouse brain atlas (12) the anterior bouton cloud is located in the ventral lateral nucleus (14). However, we could not find a cytoarchitectural border between the anterior cloud area and the PO (Figs. 1 *D* and *E* and 2*A*). Furthermore, according to the *Allen Mouse Brain Reference Atlas* (13), this anterior target area is part of the PO. We therefore suggest that the anterior bouton cloud is within the PO and refer to it as the "anterior PO" (POa). Thus, L5B in the BC targets four areas in the dorsal thalamus: the POa, POm_{medial}, $POm_{lateral}$, and PoT.

Each PO subnucleus had a characteristic 3D organization of L5B boutons. First, the $POm_{lateral}$ had the highest bouton

Table 1. Projection parameters for each target area

Nucleus	Coordinates in mm from bregma L	P	V	Interquartile summary statistics	Bouton diameter, µm GFP	mO	Boutons per L5B neuron	Boutons per column	Volume per L5B neuron, 10^{-4} mm^3	Volume per column, 10^{-4} mm^3	Bouton density, 10^{-4}/mm^3	Soma density, 10^{-4}/mm^3	Boutons per soma	Overlap, %	Map orientation (L/A/V)	Rows (A–E)	Arcs (1–6)
POa	1.0	1.3	3.2	**Median**	**2.58**	**2.86**	**5.8**	**263**	**0.6**	**24.4**	**7.0**	**3.26**	**2.2**	**60.3**	L	−0.23	−0.16
				Q1	2.33	2.56	3.4	120	0.4	18.0	6.0	2.54	1.9	26.7	A	−0.59	-0.99
				Q3	2.95	3.15	16.0	384	1.3	47.1	12.3	4.69	3.8	63.6	V	0.70	0.02
$POm_{lateral}$	1.4	2.0	3.3	**Median**	**2.88**	**3.20**	**24.4**	**1,027**	**1.1**	**32.0**	**36.5**	**4.50**	**8.1**	**18.7**	L	−0.21	−0.82
				Q1	2.56	2.86	16.7	707	0.6	25.3	18.4	3.90	4.1	13.2	A	0.38	0.55
				Q3	3.40	3.65	53.3	1,551	1.6	47.2	47.0	4.86	10.4	23.0	V	0.90	−0.14
POm_{med}	0.8	1.7	3.2	**Median**	**2.64**	**2.88**	**6.0**	**223**	**0.5**	**15.4**	**14.9**	**4.50**	**3.3**	**21.0**	L	−0.45	0.94
				Q1	2.33	2.58	3.3	140	0.2	10.9	12.2	3.58	2.7	17.8	A	0.26	0.30
				Q3	3.04	3.26	9.1	265	0.7	29.3	24.5	5.30	5.4	26.5	V	0.86	0.15
PoT	0.9	2.3	3.3	**Median**	**2.56**	**2.73**	**9.3**	**319**	**1.7**	**63.9**	**3.5**	**4.89**	**0.7**	**43.9**	L	−0.20	0.63
				Q1	2.24	2.44	2.9	95	0.6	26.9	2.3	3.53	0.5	32.9	A	0.58	0.73
				Q3	2.88	3.15	13.8	399	3.7	118.9	6.9	5.56	1.4	64.9	V	0.79	0.27
ZI	1.3	2.4	4.3	**Median**	**2.31**	**2.58**	**17.9**	**483**	**5.0**	**161.0**	**2.6**	**2.23**	**1.2**	**58.3**	L	−0.93	−0.34
				Q1	2.05	2.31	4.6	223	3.0	109.1	1.6	1.33	0.7	47.0	A	0.02	0.43
				Q3	2.58	2.86	28.3	557	13.7	263.8	3.6	2.65	1.6	75.0	V	0.36	0.83
APT	0.8	2.7	3.1	**Median**	**2.44**	**2.64**	**29.5**	**1,003**	**2.2**	**67.7**	**9.2**	**4.31**	**2.1**	**29.8**	L	−0.44	0.94
				Q1	2.24	2.44	10.7	415	0.7	30.3	7.9	1.85	1.8	25.2	A	−0.74	−0.21
				Q3	2.73	2.95	43.5	1,551	3.7	131.0	19.8	6.02	4.6	34.2	V	0.50	0.28

Summary of parameters of L5B projections to the six target nuclei in thalamus and anterior midbrain with medians (bold) and first (Q1) and third (Q3) quartiles, where applicable. Coordinates are equivalent to the mouse brain atlas (12). Diameters are affected by the fluorophore [GFP or mOrange (mO)]. Map orientations are given as unit vectors in the cardinal directions: lateral (L), anterior/posterior (A/P), and ventral (V). Procedures of calculations are given in *SI Materials and Methods*.

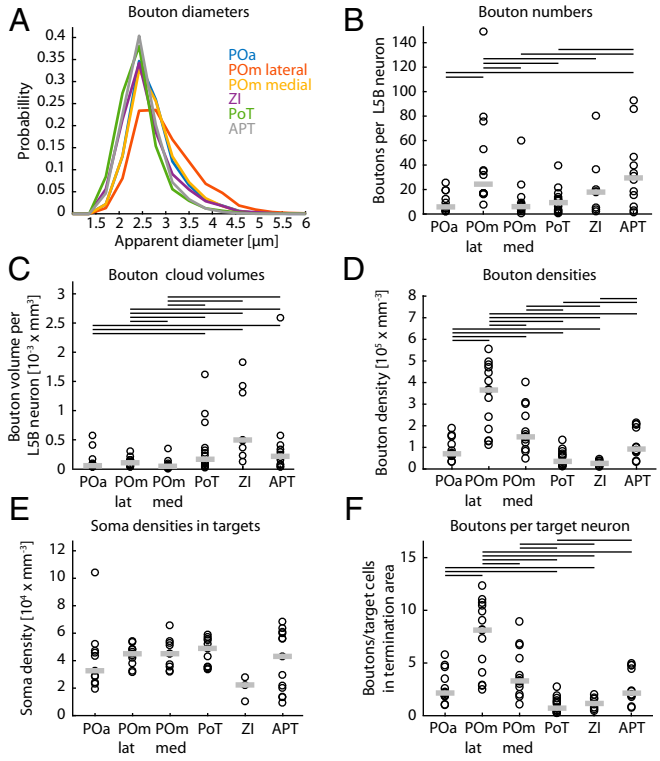

Fig. 4. Quantification of projection parameters. Parameter estimates of L5B subcortical projections for each target nucleus. (*A*) Probability histogram of bouton diameters (only GFP-labeled) in the different nuclei as indicated by different colors. (*B–F*) The value for each experiment (both GFP and mOrange) is represented by black circles, and the median of all experiments is represented by gray lines. Black lines at the top of the panel indicate which nuclei are significantly different from each other (Wilcoxon signed rank test, $P < 0.05$). (*B*) The number of boutons in different nuclei, normalized by the number of labeled L5B neurons (median = 91 L5B neurons; Q_1: 50, Q_3: 141). (*C*) Bouton cloud volumes in different nuclei normalized by the number of labeled L5B neurons (median = 91 L5B neurons; Q_1: 50, Q_3: 141). (*D*) Bouton cloud densities (the ratio of bouton number to cloud volume). (*E*) Soma densities from NeuroTrace staining measured in a subsample of sections in two experiments. (*F*) The number of boutons per target cell (ratio of bouton densities to neuron densities).

densities; bouton densities in the PoT and POa were significantly lower (Fig. 4*D*). Second, the precision and orientation of the corticothalamic maps were specific for each PO subnucleus (Fig. 5*C*). As a consequence, the PO contains four differently oriented whisker maps (Fig. 6). It remains unclear if the cortical projections into the four PO subnuclei are paralleled by inputs from other sources. For example, the spinal trigeminal nucleus interpolaris innervates only approximately one third of the PO, but whether this pathway targets specific PO subnuclei cannot be derived from the dataset (21). Previous physiological studies also hint at functionally different populations in the PO (21, 22).

L5B Projection Organization. We used the relative locations of viral deposits in the BC and respective relative bouton cloud locations to estimate the organization and precision of whisker maps in the target areas.

In the PO subnuclei, projection arcs were oriented in approximately the ventral direction (i.e., C3 projections were located ventrally of C2 projections). Projection rows, in contrast, always pointed in the direction of the PO center (e.g., the A-row projections surround those from row B) (Fig. 6). However, the very center of the PO did not receive boutons from the BC (Fig. S6). In accordance with receptive field mapping (8), we hypothesize that the PO center region receives cortical input from somatosensory cortex corresponding to the rest of the body. We found target specificity not only for map orientation but also for somatotopic precision. Although dual virus deposits in the BC were nonoverlapping, subcortical bouton clouds overlapped to a certain degree. Comparing all four PO subnuclei, we found that the POa and PoT had the highest projection overlaps and therefore received less precise somatotopic L5B input. The $POm_{lateral}$ and POm_{medial} had the lowest percentage of overlaps (~20%) and thus had the highest projection precision. This result is in accordance with previously reported corticothalamic projection map specificity (including L6) to the $POm_{lateral}$ that was suggested to be similar to that of the VPM (26). Another study, in which adjacent barrel columns were labeled (11), indicated no discernable somatotopy from the BC to the $POm_{lateral}$. These different results suggest that viral deposits at various distances within the BC together with 3D reconstructions of giant bouton clouds are necessary to reveal the somatotopic organization.

In addition to the PO, L5B also projects substantially to the GABAergic nuclei ZI and APT (2). Although both nuclei received similar numbers of boutons per L5B neuron, the APT received denser bouton clouds, with a clear somatotopic projection map in the horizontal plane. In the dorsal ZI, the L5B bouton clouds were distributed in large volumes with low density and low somatotopic precision. Both nuclei send GABAergic projections to many brain areas, including the PO, allowing complex cortico–subcortical interactions (2, 23, 24).

In summary, in all target nuclei investigated we found largely segregated L5B bouton clouds and projection maps that were predictable from the relative locations of virus deposits in the BC, together demonstrating somatotopic organization of L5B subcortical pathways. Consequently, L5B transfers multiple symmetry- and rotation-modified whisker maps from the BC to the thalamus and the anterior midbrain. The partial overlap of projections indicates some intermixing of the parallel pathways. However, whether individual postsynaptic neurons sample all available boutons from a few barrel columns or instead have a selection bias to specific origins awaits confirmation on the ultrastructural level. Thus, the L5B projection mapping points to a labeled lines organization, but the exact specificity of these labels, i.e., the exact set of encoded whiskers, depends on the innervation model, which here is assumed to be random. On anatomical grounds, a labeled lines organization aligns with previous functional studies, which revealed that $POm_{lateral}$ neurons respond to a specific set of two to four whiskers (8) resulting from cortical L5B giant bouton input (7, 18).

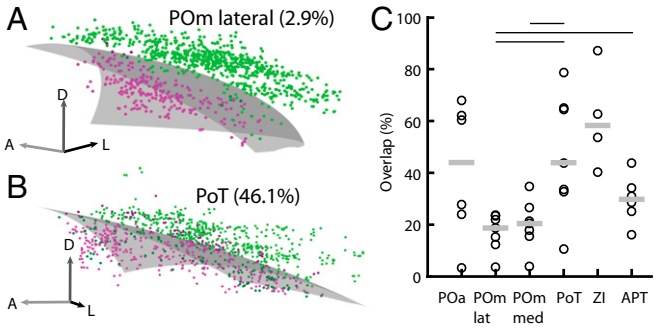

Fig. 5. Overlap between GFP- and mOrange-labeled bouton clouds calculated with GLMs. (*A*) A low-overlap example from the $POm_{lateral}$ showing a randomly selected subset of 1,000 boutons for clarity. The transparent gray surface illustrates the GLM-modeled surface that gives the best separation of bouton clouds (green and magenta dots). Overlap boutons are plotted in a dark shade of green and magenta, respectively. The percentage of boutons in the overlap volume is proportional to cloud overlap. (*B*) As in *A* but showing a high-overlap example from the PoT. (*C*) Estimated overlaps for all target nuclei. Each circle represents one experiment; gray bars show the median. Lines above the panel indicate which target nuclei are significantly different from each other (Wilcoxon signed rank test, $P < 0.05$).

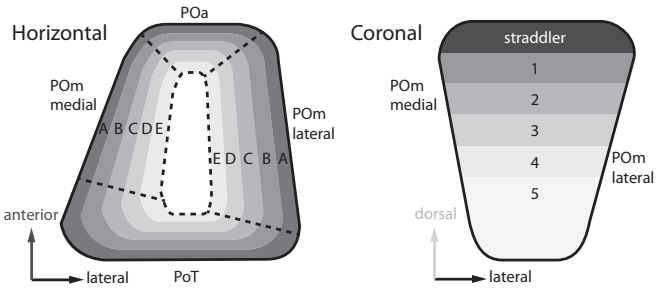

Fig. 6. PO whisker projection maps. Schematic drawings of L5B-derived whisker maps in the PO in horizontal (*Left*) and coronal (*Right*) views showing the outside–in organization of whisker rows and the dorsoventral orientation of whisker arcs. Rows and arcs are shown in shades of gray.

Corticothalamic Convergence and Divergence. We estimate that one L5B neuron supplies on average 24.4 boutons to the $POm_{lateral}$, comparable to previously published single-neuron tracing estimates in the rat (5). However, L5B projection neurons are probably an inhomogeneous population in terms of target specificity (5). The fractions of L5B neurons projecting to particular target areas and not to others influence our quantitative estimates of the number of boutons per L5B neuron. As a first approximation, we report values under the assumption that all labeled L5B neurons project to all targets.

The number of cortical neurons converging onto a single subcortical target neuron (convergence) and the number of subcortical target neurons innervated by one cortical neuron (divergence) are hitherto untested. In the $POm_{lateral}$, on average 8.1 L5B boutons are supplied to each target neuron, based on the ratio between labeled bouton and soma densities. Because of the overlap of corticothalamic projections, however, it can be assumed that additional unlabeled boutons are also present; thus 8.1 boutons is a lower-bound estimate. Because several boutons of the same L5B axon can innervate a $POm_{lateral}$ dendrite, it is likely that single L5B neurons connect to $POm_{lateral}$ neurons with more than one bouton. Recent functional convergence estimates of the pathway suggested on average ≈2.5 independent L5B inputs (7). Because multiple contacts of the same L5B neuron with a POm neuron appear as a single functional input in physiological experiments, the results can be combined to the following convergence estimate: on average, 2.5 L5B neurons (7) provide a minimum of 8.1 giant boutons contacting the postsynaptic POm neuron, resulting in at least 3.2 (8.1/2.5) giant boutons between individual L5B and $POm_{lateral}$ neurons.

Setting those 3.2 giant boutons between individual neurons in relation with 24.4 boutons per labeled L5B neuron in the $POm_{lateral}$, an average L5B neuron is estimated to innervate at most 7.5 (24.4/3.2) neurons in the $POm_{lateral}$. These estimates suggest very low divergence and convergence, indicating that the L5B-to-POm pathway is sparse and highly parallelized.

The data presented here suggest that L5B neurons of the BC are the origin of a subcortical signal pathway organized by "labeled lines" with mostly parallel and topographic projections but some mixing. In concert with a dense quadruple innervation field of the higher-order nucleus PO, the spike output from L5B in the BC is broadcast with high functional efficacy and anatomical precision via PO's widespread cortical projections (2, 27) to other cortical and subcortical areas.

Materials and Methods

All experiments were done according to the guidelines of German animal welfare and were approved by the ethical committees of the Technical University of Munich. Small deposits of two different AAVs (encoding Synaptophysin fused to GFP or mOrange) were targeted to L5B in the BC of seven mice. Next, we obtained slices of the thalamus and anterior midbrain, which were imaged by mosaic confocal microscopy. We reconstructed the location of labeled giant L5B boutons in the target areas to quantify the organization of cortico–subcortical L5B innervation. Values are provided as the median and first and third quartiles if not specified otherwise. Details about materials, surgery, microscopy and analysis are presented in *SI Text*.

ACKNOWLEDGMENTS. We thank Arthur Konnerth for providing laboratory space and infrastructure and Thomas Misgeld for providing access to his confocal microscope setup. This work was funded by Boehringer Ingelheim Fonds (A.S.), the Max Planck Society, and DFG Collaborative Research Center 1158, as well as DFG Grants 3757/3-1 and 3757/2-1 (to A.G.).

1. Woolsey TA, Van der Loos H (1970) The structural organization of layer IV in the somatosensory region (SI) of mouse cerebral cortex. The description of a cortical field composed of discrete cytoarchitectonic units. *Brain Res* 17:205–242.
2. Bosman LWJ, et al. (2011) Anatomical pathways involved in generating and sensing rhythmic whisker movements. *Front Integr Nuerosci* 5:53.
3. Sherman SM (2016) Thalamus plays a central role in ongoing cortical functioning. *Nat Neurosci* 19:533–541.
4. Bourassa J, Pinault D, Deschênes M (1995) Corticothalamic projections from the cortical barrel field to the somatosensory thalamus in rats: A single-fibre study using biocytin as an anterograde tracer. *Eur J Neurosci* 7:19–30.
5. Veinante P, Lavallée P, Deschênes M (2000) Corticothalamic projections from layer 5 of the vibrissal barrel cortex in the rat. *J Comp Neurol* 424:197–204.
6. Groh A, de Kock CPJ, Wimmer VC, Sakmann B, Kuner T (2008) Driver or coincidence detector: Modal switch of a corticothalamic giant synapse controlled by spontaneous activity and short-term depression. *J Neurosci* 28:9652–9663.
7. Mease RA, Sumser A, Sakmann B, Groh A (2016) Corticothalamic spike transfer via the L5B-POm pathway in vivo. *Cereb Cortex* 26:3461–3475.
8. Diamond ME, Armstrong-James M, Ebner FF (1992) Somatic sensory responses in the rostral sector of the posterior group (POm) and in the ventral posterior medial nucleus (VPM) of the rat thalamus. *J Comp Neurol* 318:462–476.
9. Meyer HS, et al. (2010) Cell type-specific thalamic innervation in a column of rat vibrissal cortex. *Cereb Cortex* 20:2287–2303.
10. Woolsey TA, Welker C, Schwartz RH (1975) Comparative anatomical studies of the SmL face cortex with special reference to the occurrence of "barrels" in layer IV. *J Comp Neurol* 164:79–94.
11. Wright AK, Norrie L, Arbuthnott GW (2000) Corticofugal axons from adjacent "barrel" columns of rat somatosensory cortex: Cortical and thalamic terminal patterns. *J Anat* 196:379–390.
12. Franklin KBJ, Paxinos G (2012) *Paxinos and Franklin's The Mouse Brain in Stereotaxic Coordinates* (Academic, New York).
13. Oh SW, et al. (2014) A mesoscale connectome of the mouse brain. *Nature* 508:207–214.
14. Zakiewicz IM, Bjaalie JG, Leergaard TB (2014) Brain-wide map of efferent projections from rat barrel cortex. *Front Neuroinform* 8:5.
15. Liao CC, Chen RF, Lai WS, Lin RCS, Yen CT (2010) Distribution of large terminal inputs from the primary and secondary somatosensory cortices to the dorsal thalamus in the rodent. *J Comp Neurol* 518:2592–2611.
16. Meyer HS, et al. (2013) Cellular organization of cortical barrel columns is whisker-specific. *Proc Natl Acad Sci USA* 110:19113–19118.
17. Nelder JA, Wedderburn RWM (1972) Generalized linear models. *J R Stat Soc Ser A* 135:370–384.
18. Mease RA, Sumser A, Sakmann B, Groh A (2016) Cortical dependence of whisker responses in posterior medial thalamus in vivo. *Cereb Cortex* 26:3534–3543.
19. Yu C, Derdikman D, Haidarliu S, Ahissar E (2006) Parallel thalamic pathways for whisking and touch signals in the rat. *PLoS Biol* 4:e124.
20. Moore JD, Mercer Lindsay N, Deschênes M, Kleinfeld D (2015) Vibrissa self-motion and touch are reliably encoded along the same somatosensory pathway from brainstem through thalamus. *PLoS Biol* 13:e1002253.
21. Groh A, et al. (2014) Convergence of cortical and sensory driver inputs on single thalamocortical cells. *Cereb Cortex* 24:3167–3179.
22. Gauriau C, Bernard JF (2004) Posterior triangular thalamic neurons convey nociceptive messages to the secondary somatosensory and insular cortices in the rat. *J Neurosci* 24:752–761.
23. Urbain N, Deschênes M (2007) Motor cortex gates vibrissal responses in a thalamocortical projection pathway. *Neuron* 56:714–725.
24. Giber K, et al. (2008) Heterogeneous output pathways link the anterior pretectal nucleus with the zona incerta and the thalamus in rat. *J Comp Neurol* 506:122–140.
25. Wimmer VC, Bruno RM, de Kock CPJ, Kuner T, Sakmann B (2010) Dimensions of a projection column and architecture of VPM and POm axons in rat vibrissal cortex. *Cereb Cortex* 20:2265–2276.
26. Alloway KD, Hoffer ZS, Hoover JE (2003) Quantitative comparisons of corticothalamic topography within the ventrobasal complex and the posterior nucleus of the rodent thalamus. *Brain Res* 968:54–68.
27. Mease RA, Metz M, Groh A (2016) Cortical sensory responses are enhanced by the higher-order thalamus. *Cell Reports* 14:208–215.
28. Groh A, et al. (2010) Cell-type specific properties of pyramidal neurons in neocortex underlying a layout that is modifiable depending on the cortical area. *Cereb Cortex* 20:826–836.
29. Mease RA, Krieger P, Groh A (2014) Cortical control of adaptation and sensory relay mode in the thalamus. *Proc Natl Acad Sci USA* 111:6798–6803.
30. Edelsbrunner H, Kirkpatrick D, Seidel R (1983) On the shape of a set of points in the plane. *IEEE Trans Inf Theory* 29:551–559.
31. Efron B (1979) Bootstrap methods: Another look at the jackknife. *Ann Stat* 7:1–26.